

Journal of Materials Chemistry C

Accepted Manuscript



This is an *Accepted Manuscript*, which has been through the Royal Society of Chemistry peer review process and has been accepted for publication.

Accepted Manuscripts are published online shortly after acceptance, before technical editing, formatting and proof reading. Using this free service, authors can make their results available to the community, in citable form, before we publish the edited article. We will replace this *Accepted Manuscript* with the edited and formatted *Advance Article* as soon as it is available.

You can find more information about *Accepted Manuscripts* in the [Information for Authors](#).

Please note that technical editing may introduce minor changes to the text and/or graphics, which may alter content. The journal's standard [Terms & Conditions](#) and the [Ethical guidelines](#) still apply. In no event shall the Royal Society of Chemistry be held responsible for any errors or omissions in this *Accepted Manuscript* or any consequences arising from the use of any information it contains.

ARTICLE

A ZnO/Poly(N-vinylcarbazole) Coaxial Nanocable for White-Light Emissions

Cite this: DOI: 10.1039/x0xx00000x

Shih-Shou Lo*, Li Yang and Chi-Pin Chiu

Received,
Accepted

DOI: 10.1039/x0xx00000x

www.rsc.org/

A new type of light emitting nanorods that emit white light is reported. In this study, we demonstrated an inorganic-organic coaxial nanocable fabricated through facile-coating of organic molecules on an inorganic nanorod. The coaxial nanocable consists of a unique core (ZnO nanorod) and a shell (poly(N-vinylcarbazole) PVK). Our experimental results revealed that the combined contributions from the ZnO nanorod and PVK molecule resulted in white-light emissions. The spectrum of the white-light emissions covered a wide range of the visible region and the Commission Internationale de l'Eclairage coordinates of the emitted light were (0.365, 0.385). ZnO/PVK nanocables have potential applications in lighting nanodevices and in the study platform of exciton-carrier interaction.

1. Introduction:

One-dimensional (1D) nanomaterials have been the subject of intensive research because of their large specific surface areas and quantum confinement effects.¹ They are expected to play a critical role as both interconnection and functional units in the fabrication of nanoscale optoelectronic devices. Over the decades, the core shell 1D heterostructures have attracted a great deal of interest because they allow fine control over the properties of nanomaterials. For advanced applications, combining several materials into 1D nanomaterial is an effective method of developing systems possessing desirable physical and chemical properties.²⁻⁴ However, based on a review of the literature, few studies have investigated the preparation of inorganic/organic coaxial nanocables.

Today, the production of white-light emissions is a promising area of luminescence studies. Non-covalent and energy-transfer design principles have been elegantly combined to achieve white-light-emitting organic assemblies in gels,⁵ nanoparticles,⁶ nanotubes,⁷ solvent/matrix liquid inks,⁸ excitation energy transfer.⁹ However, retaining pure white-light emissions on solid substrate is crucial for fabricating devices by transferring organic assemblies from solution. Solvent drying result in subtle changes in molecular organization, leading to impure white-light; retaining pure-white light has thus been a challenge.

ZnO, inorganic semiconductor, exhibits a direct bandgap of 3.37 eV at room temperature with a large exciton binding energy of 60 meV. The strong exciton binding energy at room temperature (26 meV) can ensure efficient exciton emissions at room temperature at low excitation energy. Consequently, ZnO is recognized as a promising photonic material in the blue-UV

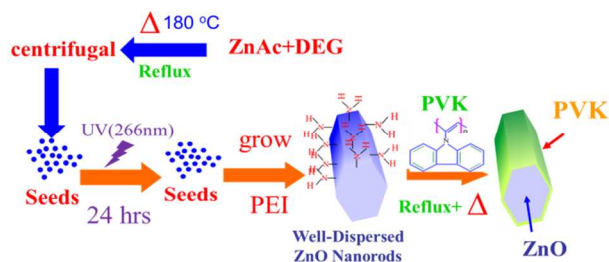
region.^{10,11} The strong and broad defect luminescence in ZnO suggests that a large part of radiative recombination occurs through in deep center. PVK (N-vinyl carbazole) is an organic semiconducting polymer that facilitates holes transport. The highest occupied molecule orbital (HOMO) and the lowest unoccupied molecule orbital (LUMO) energy of PVK are -5.5 and -2.0 eV, respectively. PVK has a strong blue emitting singlet excited-state that peaks at approximately 420 nm.¹² It has been widely used as an electronic and optical material.^{13,14}

In this paper, we report the preparation of a well-dispersed inorganic/organic nanocable (ZnO/PVK nanocable). The nanocable consists of a unique core (composed of an optically active ZnO nanorod) and a shell (composed of a layer of PVK for holes transport). White-light emissions were obtained from the ZnO/PVK coaxial nanocables. The coaxial nanocable was compared with white-light-emitting diodes (WLEDs) of standard configurations that were produced by exciting multiphosphors by UV LEDs, mixing blue LEDs with yellow phosphors, and blending multi-LEDs. The ZnO/PVK coaxial nanocables have potential applications in nanodevices for the purposes of conserving energy and miniaturization.

2. Results and Discussions

The process involved in synthesizing the ZnO/PVK nanocables plotted in Schema 1. To grow wurtzite ZnO nanorods, the seeds of ZnO nanorods were activated by using UV (266 nm) light and the growth direction of the ZnO nanorods was controlled by varying the PEI concentration.¹⁵ In order to form coaxial nanocables with well-defined interfaces, the pre-treated ZnO nanorods were thoroughly purified several times by using deionized water and ethyl alcohol. This procedure ensured the

complete removal of surface-adsorbed un-reactive complexes, as shown in Fig. 1(a). When the reaction process was complete, the nanorods were coated with PVK (Fig. 1(b)).



Scheme 1. Schematic synthesis process of ZnO/PVK coaxial nanocable

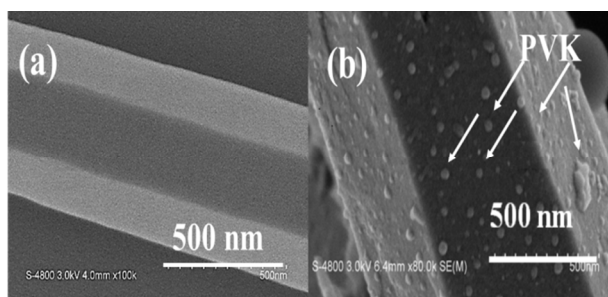


Fig. 1 (a) SEM image of as-synthesized ZnO nanorods. (b) SEM image of ZnO/PVK

The X-ray diffraction (XRD) structures of ZnO/PVK nanocables were studied and are displayed in Fig. 2. For comparison, the XRD spectra of ZnO and PVK are also displayed. Five XRD peaks were observed in the spectra of the ZnO nanorods. These strong and clear peaks revealed the high purity and crystallinity of the ZnO nanorods that were obtained. All the peaks attributed to the wurtzite ZnO structure were determined according to JCPDS card file No. 36-1451.¹⁶ No peaks characteristic of metallic Zn were observed in the XRD patterns. The XRD pattern obtained from PVK powder was similar to that reported previously,¹⁷ two diffraction peaks centered at $2\theta = 20.45^\circ$ (4.331 Å), and 7.23° (11.50 Å) were observed (the magnitudes in the brackets parentheses represent the corresponding spacing (d) value for the peak at 2θ peak).

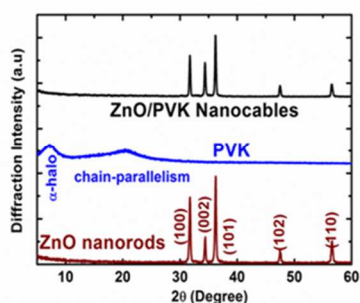


Fig. 2 XRD spectra of ZnO nanorods, PVK, and the ZnO/PVK coaxial nanocables

The former peak was a broad, diffuse, and amorphous halo whereas the latter peak was determined to be a function of the chain parallelism of PVK's. This result indicated that the structure of PVK bulk is regular in certain region. Five peaks displayed in the XRD spectra of ZnO/PVK nanocable were attributed to the ZnO nanorods' XRD signals. The disappearance of PVK XRD signals in the ZnO/PVK nanocables was attributed to the grafting of PVK molecules onto the surface of ZnO nanorods. Re-arranging PVK molecules caused the XRD peaks of PVK powder to disappear.

Figure 3(a) shows a TEM image of the as-synthesized ZnO/PVK nanocable. The ripple-like contrast observed in the TEM image caused by the PVK attached to the surface of the ZnO nanorods. A high-resolution TEM (HRTEM) image of the ZnO/PVK nanocable is shown in Fig. 3(b). Selected-area electron diffraction (SAED) measurement was performed to confirm the crystal structure of the PVK and ZnO nanorods. The SAED patterns of the areas marked in 1 and 2 in the Fig. 3(b) are shown in Figs. 3(c) and 3(d). The HRTEM image revealed that the ZnO nanorods exhibit clear lattices, indicating effectively crystallized structures. This spacing was assigned to (002) of ZnO (3.36 Å). Amorphous polymer layers can be observed in the TEM images of these samples, although the layers do not uniformly cover the surfaces of the ZnO nanorods. We confirmed that the outer layer and the inner core of the nanocables were PVK and ZnO nanorods, respectively, based on nanocable diffraction patterns; the inner core exhibited the high diffraction intensity of ZnO nanorods and the outer layer exhibited the amorphousness of PVK.

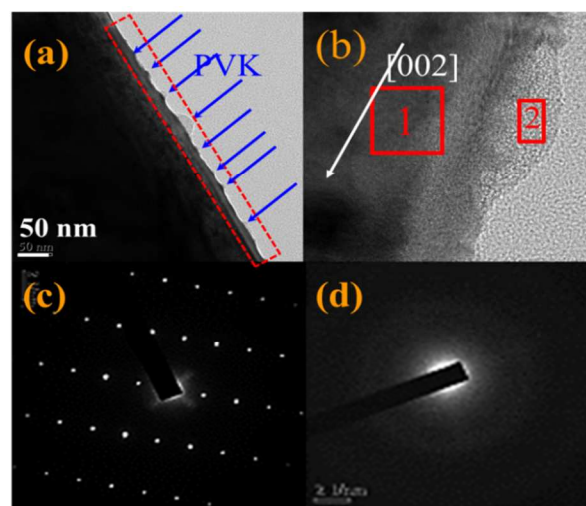


Fig. 3 (a) TEM image of ZnO/PVK nanocables. (b) HRTEM image of ZnO/PVK nanocable. (c) SAED pattern of marked area 1 in Fig. 3(b). (d) SAED pattern of marked area 2 in Fig. 3(b).

The functional groups of the as-synthesized ZnO/PVK nanocables were determined using Fourier transform infrared (FTIR) spectroscopy in the 400 to 4000 cm^{-1} range. For

comparison, the FTIR spectra of the PVK and ZnO nanorods are presented in Fig. 4. The spectra of the ZnO nanorods showed a high absorption broad-band that was approximately $\sim 540\text{ cm}^{-1}$; because of the stretching of the zinc and oxygen bonds. Previous research has located the ZnO peak between 480 cm^{-1} .¹⁸ The ZnO peaks of all samples shifted consistently because the ZnO nanorods varied in size and because ZnO nanorods are rich in zinc.¹⁹ The characteristic band of PVK was consistent with that reported in the literature.²⁰ The broad absorption in the range of $3300\text{ to }3700\text{ cm}^{-1}$ was ascribed to the existence of hydroxyl groups on the surfaces. Furthermore, three absorption peaks in the range of $2885\text{ to }3125\text{ cm}^{-1}$, $1438\text{ to }1445\text{ cm}^{-1}$ and 1320 cm^{-1} was observed; these were ascribed to C-H bonding. The strong absorption peaks at approximately 1659 cm^{-1} in Fig. 5 were ascribed to C-O bonding. The peak located at 740 cm^{-1} was ascribed to the out-of-plane C-H deformation of aromatic ring.²¹ The band at $1700\text{--}1800\text{ cm}^{-1}$ disappeared because the PVK complex was decomposed at the same time that an additional reaction occurred; this facilitated an increase in the relative intensity of the bands at $550\text{ to }560\text{ cm}^{-1}$ in the spectra of the ZnO/PVK nanocables.

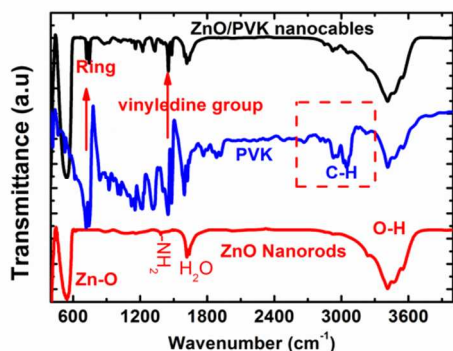


Fig. 4 FTIR spectra of ZnO nanorods, PVK, and the ZnO/PVK coaxial nanocables.

To determine the PVK contents in the ZnO/PVK nanocable, thermogravimetric analysis (TGA) experiments were conducted with a heating rate of $10\text{ }^{\circ}\text{C}/\text{min}$ in the presence of nitrogen. For comparison, the TGA data of pure PVK and ZnO are also displayed, as shown in Fig. 5(a). Thermal properties of pure ZnO remained highly stable up to $550\text{ }^{\circ}\text{C}$. For the pure PVK, the TGA thermogram exhibited a two-step degradation process, which starts with a slight steady loss at around $\sim 200\text{ }^{\circ}\text{C}$ due to degradation of the PVK chains and ends with the sudden drop at $\sim 410\text{ }^{\circ}\text{C}$ attributed to the polymer back bone degradation²². Compared to PVK and ZnO, $\sim 10\text{ mass }%$ incorporation of PVK in ZnO/PVK nanocables was obtained. By comparing the TGA weight loss of ZnO/PVK nanocable samples with that of purified ZnO and PVK as well, the PVK $\sim 12\text{ wt.}%$ of the ZnO/PVK derivatives was estimated. Detail comparing the TGA data between ZnO mix PVK and ZnO/PVK nanocable, it can be seen that there is a shift to higher PVK back bone degradation temperature for the ZnO/PVK nanocables as compared to the pure PVK, as shown on Fig. 5(b). Moreover, the PVK chains degradation process at around $\sim 210\text{ }^{\circ}\text{C}$ in the

TGA data of ZnO/PVK nanocable did not be observed due to the PVK chains have effectively bonded on the surface of ZnO nanorods by hydrogen or covalent bonding. The thermal stability improvement of PVK due to the higher thermal conductivity of ZnO nanorods that function as heat dissipated within the nanocable.

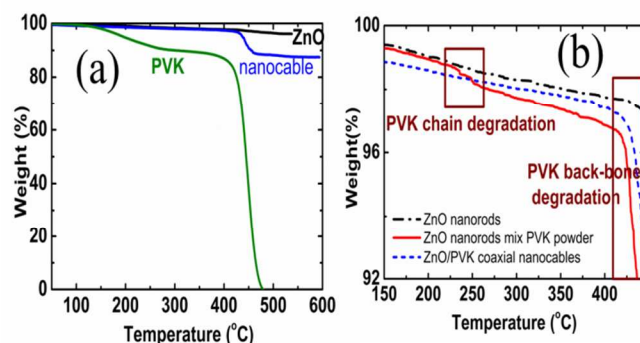


Fig. 5 (a) The weight loss curves of PVK, ZnO/PVK nanocable, and ZnO. (b) The weight loss curve of ZnO mixed PVK and ZnO/PVK nanocable. Experiments were carried out in nitrogen. Scanning rate: $5\text{ }^{\circ}\text{C min}^{-1}$. The marked area indicates the PVK chain degradation.

X-ray photoelectron spectroscopy (XPS) measurements were conducted to identify the composition and binding energy of the samples. Figs. 6(a)–6(d) presents the O1s, N1s, C1s, Zn2p3 and Zn2p1 XPS spectrum obtained from pure PVK, as-synthesized ZnO nanocables and ZnO/PVK coaxial nanocables. For the chemical analysis the main component of the C 1s and N1s spectrum is used as pure PVK reference for the other binding energies, since this value corresponds to the well-known hydrocarbon binding energy situated at 285 eV ²³ and nitrogen 400.4 eV .²⁴ It can be seen that C 1s can be decomposed into at least three components (C–C, C–N, C–OH)²⁵ in the case of pure PVK (Fig. 6(a)). The peak position of N1s (Fig. 6(b)) is located at 399 eV indicating chemical states of nitrogen in the PVK powder.²⁶ Clearly, the intensity of nitrogen bond in ZnO/PVK nanocables is higher than that of nitrogen bond in ZnO nanorods indicating the PVK molecules were attached on the ZnO nanorods. It should be noted the N1s peak in as-synthesis ZnO nanorods was detected due to the amine group ($-\text{NH}_2$) of PEI.

The XPS core level spectra of Zn 2p3 in pure PVK, as-synthesized ZnO nanorods and ZnO/PVK coaxial nanocables are shown in Fig. 6(c). In the case of pure ZnO, the Zn 2p3 XPS peak appeared at 1021.50 eV represents the formation of Zn–O bonds²⁷ while in case of pure PVK, the Zn 2p3 peak disappear. Therefore, no zinc element was composed in the pure PVK powder. When the ZnO/PVK nanocables were fabricated, the intensity of Zn–O binding energy increased. The surface states of zinc were caused by dangle-bond of zinc atom in ZnO/PVK nanocable decrease. The XPS core level spectrum of O1s of samples is shown in Fig. 6(c). In the XPS O1s spectrum of PVK is located in 534 eV . The binding energy of O1s in PVK can be assigned for H_2O ²⁸. In the XPS O1s

spectrum of ZnO nanorods, the peak can be decomposed at least two peaks located in the 530 eV (ZnO) and 532.6 eV (O-H)²⁹. The peak of O1s redshift in ZnO/PVK nanocable may be increase the O-H bonds or H₂O in the samples.²⁹ This result are in good agreement with the peak 560 cm⁻¹ of FTIR spectra in ZnO/PVK nanocable. The detail and further study for synthesis process of ZnO/PVK coaxial nanocables will be continued.

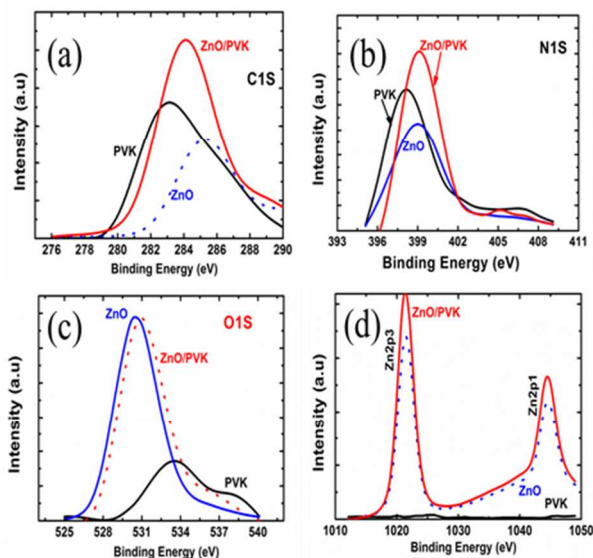


Fig. 6. XPS core-level of samples. (a) C1s (b) N1s (c) O1s (d) Zn2p3 and Zn2p1

The photoluminescence (PL) spectra of the ZnO/PVK nanocables were examined at room temperature (RT). For comparison, an RT-PL spectrum typical of ZnO nanorods grown by through a hydrothermal process (without PEI) is shown in Fig. 7(a). The RT-PL spectra for ZnO typically exhibits three major peaks: a UV near-band-edge emission peak at approximately 380 nm, a green emission peak around at approximately 510-540 nm, and a red or orange emission at approximately 600-640 nm.³⁰ The UV peak is attributed to band-edge emission, whereas the two broad, visible bands are generally attributed to deep-level defects in ZnO crystal, such as vacancies and interstitials of zinc and oxygen. In this study, neither UV nor green peaks were detected (Fig. 7(a)). Only an orange-light emission was detected in the RT-PL spectra. The orange luminescence mechanism of ZnO has been studied in the past several years and various models have been proposed. Vanheusden et al.³¹ proved that singly ionized oxygen vacancies are responsible for orange-light emissions and that these emissions results from the recombination of photo-generated holes with electrons occupying the oxygen vacancy. In our study, because ZnO nanorods were grown in a solvent in an autoclave, a quantity of O vacancies (V_O) was easily produced. We consider assumed that these nanorods have a larger surface area and more sub-surface oxygen vacancies. Therefore, it was reasonable to attribute the orange-light emissions from the ZnO nanorods in this experiment to oxygen

deficiency. This was consistent with the FTIR signal (560 cm⁻¹) of ZnO/PVK nanocable.

However, the quenching of UV light emissions (band-to-band emission) from ZnO nanorods has been reported in studies. Liu et al.³² reported a similar quenching of near-band-edge emissions from a ZnO sample upon annealing in O₂, and suggested that the expansion of the depletion layer might be attributable to a decrease of zinc vacancies within ZnO. Shalish et al.³³ reported a similar quenching of near-band-edge emissions from a size-dependent ZnO nanorod sample with a radius smaller than 30 nm. In this study, the ZnO nanorods were grown in base solvent (pH=10.7). The ZnO nanorods were larger than 30 nm (Fig. 2a) and were grown in an environment with PEI molecules. An amine groups (-NH₂) attached to the surface of the ZnO nanorods because of electron affinity.¹² When electrons are excited to from conduction bands, they are easily trapped by high-density surface states and are relaxed through a nonradiative process; thus, photon emissions occur only in the central region of the ZnO nanorods. These results can be understood based on the assumption that the type of molecule controls the number of deep-level recombination centers, or, that it induces new surface states that provide alternative non-radiative decay paths, and hence quenches PL emissions.³⁴

Pure PVK exhibited a strong emission peak at 420 nm, as shown in Fig. 7(b). This peak was assigned to the excimers of the carbazole group because the two carbazole-groups comprised a fully eclipsed, “sandwich-like” form.³⁵ The 420 nm emission light is equivalent to 2.95 eV direct band gap emission.

In the PL spectra of the ZnO/PVK nanocable, white-light emissions appeared. These white-light emissions originated from blue-light emissions at 420 nm and a visible broad band emission, as shown in Fig. 7. The decomposition of the visible band is into two peaks: 540 nm and 600 nm. However, pure PVK powder exhibited UV (420 nm) emission intensity that was substantially lower. This might be attributed to two factors. First, the weight content of the PVK in the ZnO/PVK nanocable was approximately 12 wt.% ; thus, it can be expected that the photoluminescence emission intensity of PVK was lower than that of pure PVK. Second, when PVK absorbs photons, electrons are excited into the LUMO of the shell layer and holes are left in the HOMO. Photoluminescence arises from the radiative process by which excited electrons return to valence bands. However, excited electrons were also injected into the conduction bands of the ZnO nanorods, because the conduction band of ZnO (4.2 eV) is below the LUMO of PVK (2.2 eV). The charge transfer at the interface reduced the probability of the transition of the excited electrons form LUMO to HOMO and, therefore, reduced the photoluminescence intensity. The large decrease in emission that was exhibited by the ZnO/PVK nanocables indicated that the ZnO nanorods in the prepared ZnO/PVK nanocables are effective electron trappers. The green-light emission at 540 nm were caused by the transition The orange-light emissions at 600 nm were caused by the transition of electrons from levels close

to the conduction band-edge to deeply trapped holes in the O_i^- center in the rods, as shown in Schema 2.

To investigate the luminescence properties of the ZnO/PVK nanocables in detailed, luminescence photo images of ZnO/PVK coaxial nanocable were obtained using inverted fluorescence microscopy (Olympus IX71) at various wavelengths, as shown in Fig. 8. For comparison, a photo of a ZnO/PVK coaxial nanocable under bright field conditions is also displayed in Fig. 8(b). When the ZnO/PVK nanocables were excited by UV-emission light (350 nm–380 nm), bright white-light emissions from a single ZnO/PVK nanocable were observed (Fig. 8(c)). The image by which the ZnO/PVK nanocable resulted in white-light emissions can be explained by the PL spectra of Fig. 7(b) and schema 2. The white-light emission spectrum covers a wide range of the visible region, and the Commission Internationale de l'Éclairage (CIE) coordinates of the emitted light were (0.365, 0.385), as shown in Fig. 8(a).

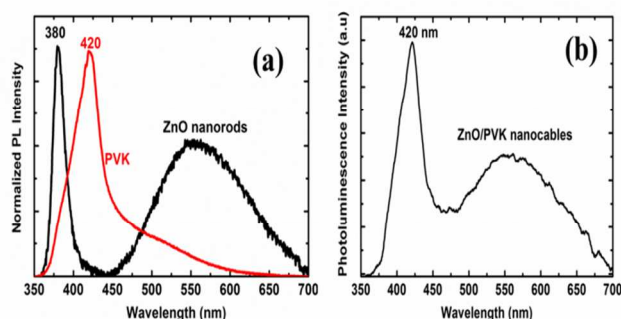
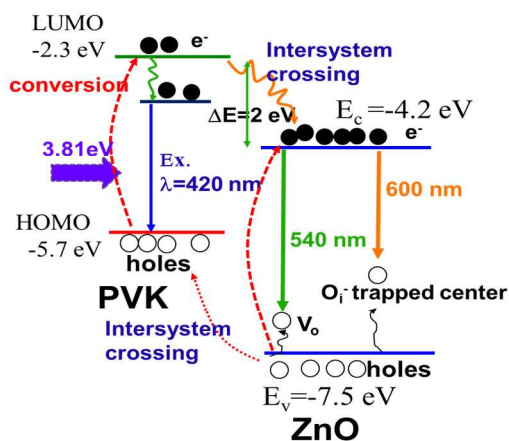


Fig. 7 (a) PL spectra of typical ZnO nanorods grown by hydrothermal process (black) and PVK (red). (b) PL spectrum of ZnO/PVK nanocables



Schema 2. Schematic diagram of ZnO/PVK coaxial nanocable light emission process under 325 nm light excitation

3. Experimental procedure

3.1. Seeds preparation of ZnO nanorods

In a primary reaction of seeds for ZnO nanorods, zinc acetate dehydrate (ZnAc, 0.04 mol) was added into 80 ml diethylene glycol (DEG). This reaction solution was heated under 170 °C. After reaching the working temperature, precipitation of ZnO spheres occurred. The intermediate product was placed in a centrifuge. After centrifuging for several minutes, the supernatant (DEG, dissolved reaction products, and unreacted ZnAc and water) was used as the stock solution. Five milliliters stock solution was dropped on a crucible. The crucible was baked with a hot-plate at 250 °C in air for 30 mins, the crucible was annealed at 550 °C in an oven for 1h. The annealed samples were pulled out from the oven for a fast cooling process. The cooling crucible was lighted by a UV (266 nm) light source for 6 hrs to active the seeds.

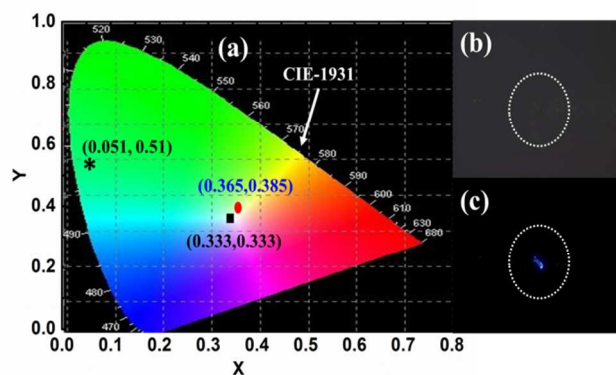


Fig. 8 (a) The CIE (1931) chromaticity diagram, with coordinate corresponding to the emission from ZnO/PVK nanocables. Also shown is the typical ZnO nanorods and equi-energy point (E) for pure white light (0.051, 0.51) and (0.333, 0.333), respectively. (b) dark field image of single ZnO/PVK coaxial nanocable. (c) Photo-image of white-light emission from single ZnO/PVK coaxial nanocable under UV light excitation

3.2. Seed preparation of ZnO nanorods

In a primary reaction of seeds for ZnO nanorods, zinc acetate dehydrate (ZnAc, 0.04 mol) was added into 80 ml diethylene glycol (DEG). This reaction solution was heated under 170 °C. After reaching the working temperature, precipitation of ZnO spheres occurred. The intermediate product was placed in a centrifuge. After centrifuging for several minutes, the supernatant (DEG, dissolved reaction products, and unreacted ZnAc and water) was used as the stock solution. Five milliliters stock solution was dropped on a crucible. The crucible was baked with a hot-plate at 250 °C in air for 30 mins, the crucible was annealed at 550 °C in an oven for 1h. The annealed samples were pulled out from the oven for a fast cooling process. The cooling crucible was lighted by a UV (266 nm) light source for 6 hrs to active the seeds.

3.3. Growth of ZnO nanorods

A hydrothermal process was used for the growth of ZnO nanorods on the as-prepared ZnO seeds. The mixing 0.05 mol/L

zinc nitrate, 0.05 mol/L hexamethylenetetramine (HMT), 60 ml/L ammonia, 8 g/L polyetherimide (PEI) and 500 ml deionized water with slowly stirring until complete dissolution in a Teflon vessel. Before being transferred to a Teflon-lined autoclave, the post-treated crucible was immersed in the solution to peel off the seeds from the crucible under an ultrasonic water bath for 5 min. The hydrothermal syntheses were conducted at 210 °C for 10 hrs in an autoclave. After the reactions, white crystalline products (well-dispersed ZnO nanorods) were harvested by centrifugation and thorough washings six-times with deionized water. Finally, the solution was dropped on a glass and heated at 120 °C for drying in air.

3.4. Synthesis of ZnO/PVK nanocables

The reflux process was used for the synthesis process of well-dispersed ZnO/PVK nanocables. A typical process, the as-fabricated ZnO nanorods and PVK was mixed at weight ratio of 1:1 in 50 ml tetrahydrofuran (THF) solution. The mixture solution was put into a three-neck flask and refluxed at 70 °C for 3 h. After the reactions, white products (well-dispersed ZnO/PVK coaxial nanocables) were harvested by centrifugation and thorough washings six-times with alcohol and deionized water. Finally, the solution was dropped on a glass and heated at 120 °C for drying in air.

3.5. Structural Characterization

XRD patterns of the films were recorded at room temperature on a D8-Advanced Bruker diffractometer with a Cu-K α ($\lambda = 1.54 \text{ \AA}$) source in Bragg-Brentano geometry using a Sol-X energy dispersive detector. Powder diffractograms were taken in an angle range from 5° to 65° using a step size of 0.02°/s and a step time of 4 s. Raman spectra up to 800 cm⁻¹ were acquired at room temperature with a LabRam spectrometer (Horiba Jobin Yvon), integration time: 150 s. per spectrum, microscope objective: 100x, and He/Ne laser (632.8 nm) as excitation source. Additional parts were an optical microscope (Olympus BX) to focus the surface of the sample, notch filter (D1.0) and a monochromator to separate Raman and Rayleigh scattering. Calibration was performed using a silicon wafer (phonon line at about 520 cm⁻¹). The morphology of the ZnO/PVK nanocables was determined using a Hitachi model H-800 transmission electron microscope (TEM). Fourier transform infrared absorption spectroscopy (FTIR) spectra were measured at room temperature on a FTIR spectrometer (PERKIN ELMER) using the KBr Pellet technique to determine the structure of the product. Photoluminescence (PL) spectra were performed at room temperature using a He:Cd laser with a wavelength of 325 nm.

4. Conclusions

We have successfully fabricated ZnO/PVK coaxial nanocable via a simple chemical process. The FTIR and XPS spectra of the ZnO/PVK coaxial nanocables indicated that PVK molecules were grafted on the surface of ZnO nanorods. The DSC curves

of ZnO/PVK nanocables revealed the thermal stability improvement of PVK due to the PVK chains were anchored on the surface of ZnO nanorods. A white-light emission was obtained from single ZnO/PVK coaxial nanocable under UV light excitation. The white-light emission spectra covered a wide range of the visible region, and the CIE coordinates of the emitted light were (0.365, 0.385). The ZnO/PVK coaxial nanocables have potential applications in lighting nanodevices and in the study platform of excitons-carriers interaction.

Acknowledgements

The author would like to thank the Ministry of Science and Technology of Republic of China, Taiwan, for financially supporting this research under Contract No. (MOST-103-2112-M-035-001-MY3).

Notes and references

Department of Photonic, Feng-Chia University, No. 100, Wenhwa Rd. Seatwen, Taichung, 40724, Taiwan, (R.O.C.)

1. Y. Gu, I. L. Kuskovsky, M. Yin, S. O'Brien and G. F. Neumark, *Appl. Phys. Lett.* 2004, **85**, 3834
2. L. J. Lauhon, M. S. Gudiksen, D. Wang, and C. M. Liber, *Nature*, 2002, **420**, 56
3. Y. Yin, Y. Lu, Y. Sun, and Y. Xia, *Nano Lett.*, 2002, **2**, 427
4. S. S. Lo, W. S. Hsu, S. H. Sie, and H. J. Leu, *J. Mater. Chem.*, 2012, **22**, 12618
5. C. Vijayakumar, V. K. Praveen, and A. Ajayaghosh, *Adv. Mater.* 2009, **21**, 2059
6. C. Giansante, C. Schafer, G. Raffy, and A. D. Guerso, *J. Phys. Chem. C*. 2012, **116**, 21706
7. Y. L. Lei, Y. Jin, D. Y. Zhou, W. Gu, X. B. Shi, L. S. Liao, and S. T. Lee, *Adv. Mater.* 2012, **24**, 534
8. S. S. Babu, J. Aimi, H. Ozawa, N. Shirahata, A. Saeki, S. Seki, A. Ajayaghosh, H. Mçhwald, T. Nakanishi, *Angew. Chem. Int. Ed.* 2012, **51**, 3391
9. K. P. Vakayil, R. Choorikkat, B. Elisa, A. Ayyappanpillai, A. Nicola *Chem. Soc. Rev.* 2014, **43**, 4222
10. X. Wang, J. Zhou, J. Song, J. Liu, N. Xu, and Z. L. Wang, *Nano. Lett.* 2006, **6**, 2768
11. W. I. Park, Y. H. Jun, S. W. Jun, and G. C. Yi, *Appl. Phys. Lett.* 2003, **82**, 964
12. B. Nowacki, E. Lamazaki, A. Cirpan, F. Karasz, D. Z. Teresa, and A. L. Akcelrud, *Polymer.* 2009, **50**, 6057
13. T. R. Hebner, C. C. Wu, D. Marcy, M. H. Lu, and J. C. Sturm, *Appl. Phys. Lett.* 1998, **72**, 519
14. N. Blouin, A. Michaud, and M. Leclerc, *Adv. Materials.*, 2007, **19**, 2295
15. L. E. Greene, B. D. Yuhas, M. Law, D. Zitoun, and P. Yang, *Inorg. Chem.*, 2006, **45**, 7535
16. W. I. Park, D. H. Kim, S. W. Jung, and G. H. Yi, *Appl. Phys. Lett.* 2002, **80**, 4232
17. Y. U. Chen, R. F. Cai, L. X. Xiao, Z. E. Huang, and R. F. Cai, *J. Poly. Sci.* 1998, **33**, 4633
18. N. Vigneshwaran, S. Kumar, A. A. Kathe, P. V. Varadarajan, and V. Prasad, *Nanotechnology* 2006, **17**, 5087

19. A. Dev, R. Niepelt, J. P. Richters, C. Ronning, and T. Voss, *Nanotechnology* 2010, **21**, 065709
20. T. Chen, G. Z. Xing, Z. Zhang, H. Y. Chen, and T. Wu, *Nanotechnology* 2008, **19**, 435711
21. P. Bertoncello, A. Notargiacomo, V. Erokhin and C. Nicolini, *Nanotechnology*, 2006, **17**, 699-705
22. C. Giansante, C. Schafer, G. Raffy, and A. D. Guerso, *J. Phys. Chem. C* 2012, **116**, 21706
23. G. L. Li, G. Liu, M. Li, D. Wan, K. G. Neoh, and E. T. Kang, *J. Phys. Chem. C*, 2010, **114**, 12742
24. B. Zaidi, S. Ayachi, A. Mabrouk, J. L. Fave, P. Molinie, M. Ghedira, and K. Alimi, *J. Appl. Poly. Sci.* 2003, **89**, 3091
25. Y. L. F. Musico, C. M. Santos, M. L. P. Dalid and D. F. Rodrigues, *J. Mater. Chem. A* 2013, **1**, 3789
26. Y. Deng, Y. Li, J. Dai, M. Lang, and X. Huang, *J. Poly. Chem.* 2011, **49**, 4747
27. K. Kotsisa and V. Staemmler, *Phys. Chem. Chem. Phys.* 2006, **8**, 1490
28. R. Bayon and C. Maffiotte, J. Herrero, *Thin Solid Films* 1999, **353**, 100.
29. N. Naseri, M. Yousefi, O. Moradlou and A. Z. Moshfegh, *Phys. Chem. Chem. Phys.* 2011, **13**, 4239
30. Zhiyong Fan, Pai-chun Chang, Jia G. Lu, Erich C. Walter, Reginald M. Penner, Chien-hung Lin and Henry P. Lee, *Appl. Phys. Lett.* 2004 **85**, 6128
31. K. Vanheusden, C. H. Seager, W. L. Warren, D. R. Tallant and J. A. Voigt, *Appl. Phys. Lett.* 1996, **68**, 403
32. D. Liu, W. Wu, Y. Qiu, S. Yang, S. Xiao, Q. Wang, L. Ding, and J. Wang, *Langmuir*, 2008, **24**, 5052
33. I. Shalish, H. Temkin, and N. Venkatesh, *Phys. Rev. B* 2004, **69**, 245401
34. M. Y. Guo, A. M. C. Ng, F. Liu, A. B. Djurišić, W. K. Chan, H. Su, and K. S. Wong, *J. Phys. Chem.* 2011, **115**, 11095
35. Y. Liu, N. Li, X. Xia, Q. Xu, J. Ge, J. Lu, *Mater. Chem. Phys.* 2010, **123**, 685